JNeurosci
THE JOURNAL OF NEUROSCIENCE

Research Articles | Behavioral/Cognitive

Subliminal beauty engages the brain's valuation circuits

https://doi.org/10.1523/JNEUROSCI.2265-25.2026

Received: 12 December 2025
Revised: 21 July 2026
Accepted: 26 August 2026

Copyright © 2026 the authors

This Early Release article has been peer reviewed and accepted, but has not been through the composition and copyediting processes.The final version may differ slightly in style or formatting and will contain links to any extended data.

Alerts: Sign up at www.jneurosci.org/alerts to receive customized email alerts when the fully formatted version of this article is published.

Subliminal beauty engages the brain's valuation circuits

Patrícia Fernandes[1], Joseph W. Kable[2], Jorge Almeida[1], Anita Tusche[3,4], Christian C. Ruff[5], & Fredrik Bergström[1,3,6]

1. CINEICC, Faculty of Psychology and Educational Sciences, University of Coimbra, Portugal.

2. Department of Psychology, University of Pennsylvania, Philadelphia, PA 19104, USA.

3. Department of Psychology, Queen's University, Kingston, ON K7L 3N6, Canada.

4. Center for Neuroscience Studies, Queen's University, Kingston, ON K7L 3N6, Canada.

5. Zurich Center for Neuroeconomics, Department of Economics, University of Zurich, Switzerland.

6. Department of Psychology, Gothenburg University, Sweden.

Corresponding author:

Fredrik Bergström

Department of Psychology, Queen's University, Kingston, ON K7L 3N6, Canada.

e-mail: f.bergstrom@protonmail.com

Running title: Subliminal beauty in aVS and vmPFC

JNeurosci Accepted Manuscript

Abstract

Neuroeconomic models propose that the anterior ventral striatum (aVS) and ventromedial prefrontal cortex (vmPFC) are key regions for computing subjective value (SV) signals that guide choice. However, the role of conscious awareness in this process remains debated. Here we examined whether SV can be automatically computed in these regions without conscious awareness. In an fMRI experiment, human participants (24 females, 5 males) viewed faces that varied in attractiveness under three conditions: (i) suppressed from awareness via continuous flash suppression (CFS), (ii) clearly visible without suppression, or (iii) absent (background only) with CFS. Participants reported trial-wise facial identity (objective) and visibility (subjective) measures of facial awareness. In a post-fMRI session, they rated the attractiveness of each face as a measure of SV. When faces were seen, task performance (d') exceeded chance and responses were faster than in absent trials. When faces were unseen, performance was at chance but responses were slower than absent trials. Neurally, seen and unseen faces elicited greater neural signal than absent trials and showed similar neural patterns in the fusiform face area (FFA). Critically, neural signal in vmPFC correlated with SV for both seen and unseen faces, with similar neural patterns. In aVS, SV-related signal was only observed for unseen faces. Furthermore, mean face-related signal in FFA correlated with SV-related signals in aVS and vmPFC for unseen faces. These findings demonstrate that SV can be automatically computed in aVS and vmPFC without conscious awareness, suggesting a neural pathway by which subliminal information can influence value-based choice.

Keywords: subliminal, beauty, subjective value, fMRI, conscious awareness

JNeurosci Accepted Manuscript

Significance statement

A central question in consciousness research and decision neuroscience is whether the brain's valuation circuitry – particularly the anterior ventral striatum (aVS) and ventromedial prefrontal cortex (vmPFC) – can compute subjective value automatically without conscious awareness. This question is important because prevailing accounts often assume that cognitive functions supported by the prefrontal cortex require conscious awareness of task-relevant information. Using continuous flash suppression and neuroimaging, we found that faces reported unseen nevertheless evoked value-related signals in aVS and vmPFC that scaled with subjective attractiveness ratings. These findings demonstrate that subjective value can be computed automatically from social information in the absence of conscious awareness.

Introduction

We may think we are aware of all the information influencing our decisions, but this intuition is likely misleading. We are only consciously aware of a fraction of our neural processes, many of which operate automatically, below our awareness. For instance, our brain seems to automatically extract useful information, such as affordances and other object properties when seeing manipulable objects (Almeida et al., 2023; Bergström et al., 2021; Valério et al., 2025); and trustworthiness, dominance features, and attractiveness when seeing faces (Engell et al., 2007; Kim et al., 2007; Miao et al., 2022). To what extent decision processes operate outside of our conscious awareness and influence our choices is not well understood and heavily debated (Newell & Shanks, 2014). This is especially true for value-based decisions, which involve evaluating and comparing options based on their subjective value (SV), an individualized estimate of their desirability or worth.

JNeurosci Accepted Manuscript

Explicit evaluation of consciously presented objects is consistently associated with a positive relationship between their SV and neural signals in aVS and vmPFC. Because these core valuation circuits represent the SV of choice options across stimuli and tasks, their activity is thought to reflect an abstract "common currency" that enables the brain to compare diverse options such as food, money, or social approval (Bartra et al., 2013; Chib et al., 2009; Kable & Glimcher, 2007, 2009; Levy & Glimcher, 2012).

Interestingly, neuroimaging research has demonstrated that SV computations can arise automatically, without explicit evaluation instructions, by presenting consciously perceived objects during passive viewing or unrelated distractor tasks. These studies found that neural signals or patterns in aVS and vmPFC correlated with SV and could predict choice (Kim et al., 2007; Lebreton et al., 2009; Levy et al., 2011; Smith et al., 2014; Tusche et al., 2010), though other work did not (Grueschow et al., 2015). A key limitation is that with consciously presented stimuli, spontaneous conscious evaluations cannot be ruled out, as they cannot be measured without potentially inducing them. Presenting stimuli subliminally addresses this by eliminating conscious evaluation.

However, subliminal stimuli introduce other methodological challenges, and studies of SV processing under such conditions are scarce, with mixed results. For example, subliminal cues linked to monetary rewards or punishments modulated aVS signal and influenced choice, suggesting subliminal valuation and learning (Pessiglione et al., 2008). Similarly, subliminal erotic compared to neutral images engaged the aVS, consistent with automatic processing of biologically relevant value (Oei et al., 2012). In contrast, other studies using subliminal images of coins (Bijleveld et al., 2014; Pessiglione et al., 2007), erotic images (Gillath & Canterberry, 2012), or facial attractiveness (Ito et al., 2015), did not find subliminal SV effects in aVS or vmPFC. Instead, when observed at all, those effects fell outside core valuation circuits and likely reflected non-SV processes. Because subliminal SV effects only were reported subcortically, conscious awareness was proposed necessary for prefrontal SV processing (Bijleveld et al., 2012).

JNeurosci Accepted Manuscript

However, none of those studies collected trial-wise awareness measures during their main experiments. Instead, awareness was inferred from group-level discrimination performance (at chance) before or after the task, which risks including trials with conscious awareness. This may explain why Pessiglione et al.'s (2008) findings were not replicated in a behavioral study that applied trial-wise awareness measures (Skora et al., 2023). Moreover, most studies used backward masking with very brief durations, which yield weaker subliminal effects than methods such as CFS or attentional blink.

We recently challenged the view that prefrontal SV processing requires conscious awareness, showing that subliminal probabilities modulate SV in vmPFC (Fernandes et al., 2025). However, because this subliminal information was task-relevant, its processing may have been top-down rather than purely automatic and bottom-up.

Here, we investigated whether SV (facial attractiveness) can be automatically computed in aVS and vmPFC without conscious awareness. We found that subliminal faces elicited SV signals in both aVS and vmPFC, indicating that SV computations can occur automatically and operate independently of conscious awareness.

Materials and Methods

Participants

We recruited 36 healthy volunteers from the University of Coimbra campus area. All participants had normal or corrected-to-normal vision, gave written informed consent, received extra course credits (if applicable), and a 20-euro reward voucher for participation. The study was approved by the Ethics Committee of the Faculty of Psychology and Educational Sciences of the University of Coimbra, Portugal.

Four participants were excluded prior to the fMRI session due to more than 20% suppression breaks during practice. Following the fMRI session, one participant was excluded for unusually high task performance (d') when faces were reported unseen (d' > 3 SD) to avoid

JNeurosci Accepted Manuscript

the possibility of conscious influences; one for irretrievable MRI data corruption; and one for insufficient unseen trials caused by frequent suppression breakthroughs (17 trials in total for all runs). In addition, one run was excluded from a participant who had only one unseen trial in that run. We therefore used 29 participants (24 females; 17 – 28 age range, M = 20, SD = 2.7 years; 3 with same-sex attraction) for our analyses.

Stimuli and Procedure

The study consisted of a 30-45 min instruction and practice session (Mdn = 28 days) prior to a 90 min fMRI session that was immediately followed by post-fMRI attractiveness ratings. The fMRI task was programmed in OpenSesame, stimuli (400 x 400 pixels, roughly subtending 7.27 degrees visual angle) was presented on a BOLDscreen 32UHD (60 Hz, 1024 x 768 resolution) (Cambridge Research Systems Ltd., UK), and responses were collected with a Cedrus Lumina button box. Stimuli were viewed through red–green anaglyph glasses to enable continuous flash suppression (CFS) during the face-identification task.

The fMRI task had 261 trials in total across three stimulus presentation conditions (Figure 1A): (i) a clearly visible face without CFS, presented in gray-scale to both eyes, superimposed on green background and moving red Mondrians (n = 72; Face + No CFS); (ii) a face rendered invisible by CFS, a green-scaled face presented to the non-dominant eye, and moving red Mondrians to the dominant eye (n = 144; Face + CFS); and (iii) absent face, a uniform green background presented to the non-dominant eye, and moving red Mondrians to the dominant eye (n = 45; No Face + CFS). When faces were presented to both eyes, they were always consciously perceived. When faces (or empty backgrounds) and Mondrians were presented to different eyes, only the Mondrians were consciously perceived, whereas the faces or backgrounds were suppressed but subliminally processed in the brain, but occasionally broke through suppression. Following prior work (Bergström & Eriksson, 2018; Fontan et al., 2021; Pedale et al., 2023), trials were categorized as seen (visible and reported seen), unseen (suppressed and reported unseen), or absent (absent and reported unseen) based on presentation condition and PAS reports.

JNeurosci Accepted Manuscript

The original face images were cropped in an oval shape to exclude non-facial features, Gaussian blur (1 pixel radius) was applied, the opacity of the face was lowered to blend in with the background, additional blur was applied to the edge around the face, the SHINE Toolbox (https://github.com/RodDalBen/SHINE_color; Dal Ben, 2023) was used to match luminance and spatial frequency while maintaining the structure of the faces, and custom Matlab code was used to make the modified face images and empty backgrounds green and to create red Mondrian images to be used for CFS (http://martin-hebart.de/webpages/code/stimuli.html; Stein et al., 2011).

Each trial (Figure 1B) consisted of: a jittered fixation cross (3 - 7 s), stimulus presentation (3 s; suppressed faces ramped in over 200 ms to reduce suppression breaks), jittered fixation dot (3 - 7 s), a match-to-sample response (match or non-match; max 4 s), perceptual awareness scale (PAS) report (1 = No visual experience of a face, 2 = vague-to-clear visual experience of a face; max 4 s; Fernandes et al., 2025; Sandberg et al., 2010). Participants were instructed to memorize the face if they saw it, and after the delay, indicate whether the sample face matched the previously presented face. They were told that a face was always presented, but mostly suppressed, and that when they did not see it, they should guess based on their gut-feeling or intuition rather than rely on systematic strategies (e.g., always pressing “non-match”). After each trial, they provided their PAS rating for the face. Importantly, the task contained no attractiveness judgments, and participants were unaware that they would later provide post-fMRI attractiveness ratings.

Immediately after scanning, participants rated the attractiveness of all 12 unique faces from the fMRI session on a 1–10 scale via Google Forms. Ratings were unrestricted in time and participants were told they could reuse ratings across faces. These ratings served as our measure of SV.

The twelve unique faces used in the experiment were pre-selected to represent three categories of attractiveness (low, medium, high), to ensure a wide distribution of subjective ratings across participants. All faces appeared in both visible and suppressed conditions, with

JNeurosci Accepted Manuscript

more repetitions in the suppressed condition. Faces in the low and medium categories were taken from the Chicago Face Database (Ma et al., 2015), corresponding to the lowest and mid-range average ratings. Because the database did not include faces at the top of the attractiveness scale, we supplemented our stimulus set with AI-generated model faces (https://generated.photos) for the high-attractiveness category. This approach ensured coverage across the full attractiveness spectrum and maximized variance for the parametric SV analyses. Participants viewed only faces of the sex they reported being most attracted to, as indicated in a pre-screening form that also included demographic, eligibility, and MRI safety questions. The reported attractiveness ratings confirmed a wide spread across the full scale, with substantial individual variability in both male and female stimulus sets (Figure 1C).

Before being scheduled for the fMRI session, participants completed a shorter practice version of the task to ensure that they understood the instructions and that continuous flash suppression (CFS) worked effectively on them. Task instructions were first provided in writing and then explained in detail by a researcher before the practice began. To secure a sufficient number of unseen trials for later analyses, only participants who saw fewer than 20% of faces during practice were invited to proceed to the fMRI session.

MRI acquisition

MRI data were acquired on a 3T MAGNETOM Vida whole-body scanner (Siemens Healthineers, Erlangen, Germany) at Hospital da Luz de Coimbra using a 32-channel head coil. Each participant completed one scanning session consisting of three functional runs (746 volumes per run; 2238 volumes and 75 min in total) with a high-resolution anatomical scan acquired between runs.

Anatomical MRI images were acquired using a T1-weighted magnetization-prepared rapid gradient echo (MPRAGE) sequence [repetition time (TR) = 2300 ms, echo time (TE) = 2.32 ms, voxel size = 0.9 x 0.9 x 0.9 mm^3, flip angle = 8 degrees, field of view (FoV) = 240 x 240, matrix size = 256 x 256, bandwidth (BW) = 200 Hz/px, GRAPPA acceleration factor 2].

JNeurosci Accepted Manuscript

Functional MRI (fMRI) data were acquired using a T2*-weighted gradient echo planar imaging (EPI) sequence (TR = 2000 ms, TE = 36 ms, voxel size = 3 x 3 x 3 mm^3, slice thickness = 3 mm, FoV = 210 x 210, matrix size = 70 x 70, flip angle = 75 degrees, BW = 1786 Hz/px). Each volume contained 50 contiguous transverse slices acquired in interleaved order, oriented parallel to the AC–PC line and tilted 30° to improve signal coverage in the vmPFC.

Preprocessing of MRI data

MRI data were preprocessed with fMRIPrep 24.0.1 default settings. For anatomical images, the T1-weighted scan was corrected for intensity non-uniformity, skull-stripped, segmented into gray matter, white matter, and CSF, and spatially normalized to MNI space via non-linear registration. For functional images, preprocessing included generation of a reference volume (custom fMRIPrep method), head-motion correction (six rigid-body parameters), and slice-time correction to middle slice. The BOLD reference was co-registered to the T1 reference image. Preprocessed BOLD series were then normalized to MNI space. 24 motion parameters, several confounding time series, and physiological noise regressors were automatically calculated by fMRIprep defaults. Finally, an 8 mm FWHM Gaussian kernel was applied with SPM12 before statistical analysis.

Statistical analysis

As in previous work (Bergström & Eriksson, 2018; Fontan et al., 2021; Pedale et al., 2023), we defined condition categories in the following way: “Seen” was defined as a visibly presented face without suppression and participants reporting a visual experience of the face (PAS = 2). “Unseen” was defined as a face presented with suppression and participants reporting no visual experience of the face (PAS = 1). “Absent” was defined as the absence of a face presented with suppression and participants reporting no visual experience of a face (PAS = 1). These three seen, unseen, and absent categories and naming convention are used for all the subsequent analysis. Trials not included in these categories were grouped into an “other” condition for fMRI modeling but otherwise not of interest.

JNeurosci Accepted Manuscript

Behavioral analysis

We looked at task performance and reaction time. Task performance (d') was defined as z(hits) minus z(FAs), where "hits" was when the to be remembered face matched the sample face and the response was "match", while "false alarms" was when the to be remembered face did not match the sample and response was "match." Prior to reaction time analysis, we removed outlier trials with a reaction time < 250 ms (e.g., accidentally pressing the button before seeing the query) or > three standard deviations from the group mean (e.g., spacing out), and log10-transformed the reaction times for a normal distribution (Ratcliff, 1993).

fMRI analysis

General Linear Model (GLM). Within-participant modeling was conducted in SPM12 using a GLM with restricted maximum likelihood estimation. The model included 14 regressors of interest: unseen face presentation, unseen linear parametric modulation of SV, unseen ISI, unseen response; seen face presentation, seen linear parametric modulation, seen ISI, seen response; absent face presentation, absent ISI, absent response; other face presentation, other ISI, other response. The "other" category contained trials that did not fit the seen, unseen, and absent categories (e.g., faces breaking suppression).

Parametric SV regressors for seen and unseen faces were modeled as linear modulations, using run-wise mean-centered and z-scored subjective attractiveness ratings from the post-fMRI session. Regressors of interest were modeled from stimulus onset to offset and convolved with the canonical hemodynamic response function. A high-pass filter with a cut-off of 128 s and a global AR(1) autocorrelation model were applied.

The GLM also contained 40 regressors of no interest: 24 head motion parameters, 4 cerebrospinal fluid (CSF) CompCor components, 11 white matter CompCor components, and one framewise displacement parameter. The number of CompCor components was equalized

JNeurosci Accepted Manuscript

across participants and runs by selecting the maximum number of components available for all participant's runs (Fernandes et al., 2025).

For multivariate analyses, a separate GLM was computed to estimate beta maps. The model included 46 regressors of interest per run: one regressor for each of the unique unseen faces presented (12 in total), one regressor for each unique seen face presented (12 in total), one regressor for each absent presentation (15 in total), ISI and response regressors separated by seen, unseen, and absent conditions (6 in total), and a "other" regressor. No parametric modulation regressors. The same 40 regressors of no interest to model motion and physiological noise as before. This procedure therefore yielded up to 12 beta maps for unseen and 12 beta maps for seen face presentations per run (36 seen and 36 unseen total per participant), as well as 15 beta maps for absent trials (45 total per participant).

Regions of interest. We focused on three a priori regions of interest (ROIs) based on previous literature. The anterior ventral striatum (aVS) and ventromedial prefrontal cortex (vmPFC) were selected because they form part of the brain's core valuation circuit, consistently associated with subjective value (SV) but not salience (for meta-analysis, see Bartra et al., 2013) and reliably engaged by facial attractiveness (for meta-analysis, see Chuan-Peng et al., 2020). The fusiform face area (FFA) was included as a high-level visual face processing region (Grill-Spector et al., 2017; Kanwisher et al., 1997).

The aVS was defined using the AAL3 anatomical atlas to ensure precise coverage of the entire region while avoiding neighboring structures, and was used for both univariate and multivariate analyses. The vmPFC was defined by placing a spherical ROI centered on the coordinates [-1, 46, -7] from Bartra et al.'s (2013) SV meta-analysis. For univariate analyses, we used a 4 mm radius sphere, while for multivariate analyses we used a 12 mm radius sphere. The FFA was defined using peak coordinates [40, -50, -20] from a NeuroSynth meta-analysis with the search term "faces," with spheres of 4 mm radius for univariate and 12 mm for multivariate analyses. We removed parts of the larger FFA spheres that crossed over to the cerebellum. We used smaller spheres in univariate analyses to target peak signal as

JNeurosci Accepted Manuscript

precisely as possible, and larger spheres for multivariate analyses to allow data-driven weighting of spatially heterogeneous signals within each ROI. The multivariate analysis also complemented the ROI-average analysis by testing whether predictive information generalized across participants.

Univariate analysis. For ROI analyses, the mean contrast estimate across all voxels in the ROI were extracted for each participant and entered into group-level t-tests. One-tailed tests were used whenever we had strong a priori hypotheses derived from previous literature (e.g., neural responses in valuation circuits should scale positively with SV), or when only one direction of the effect was meaningful (e.g., neural signal or decoding being greater than chance).

To test whether stronger face-related signal in the FFA was related to stronger SV-related signal in valuation regions during the face presentation, we correlated contrast estimates for seen faces > absent in FFA with the parametric SV estimates for seen faces in aVS and vmPFC, as well as, unseen faces > absent in FFA with the parametric SV estimates for unseen faces in aVS and vmPFC.

In addition to ROI analyses, we performed whole-brain contrasts to test for effects outside our a priori regions. These analyses were restricted to a grey matter mask and evaluated using non-parametric permutation testing (10,000 permutations) with Threshold-Free Cluster Enhancement (TFCE; http://www.neuro.uni-jena.de/tfce/; Smith & Nichols, 2009) to adjust for cluster size and voxel-wise FDR correction for multiple comparisons.

Multivariate decoding analysis. To assess out-of-sample predictions (or "decoding"), we used a Thresholded Partial Least Squares regression (T-PLS; https://github.com/sangillee/TPLSm; Lee et al., 2022) implemented in MATLAB R2022a. T-PLS was selected because it can flexibly predict both continuous and binary variables, handles high voxel collinearity, performs voxel selection within a nested cross-validation framework, is computationally efficient, and provides interpretable coefficients. We performed two main sets

JNeurosci Accepted Manuscript

of analyses: (i) binary decoding (seen face vs. absent; unseen face vs. absent; coded as 1 for face and 0 for absent) to test for face-related information in the FFA, and (ii) SV decoding as a continuous variable (for seen and unseen faces) to test for SV signal in aVS and vmPFC. We used a leave-one-participant-out cross-validation (LOPO-CV) procedure to test whether predictive information generalized across participants within ROIs, while also providing large training sets for model estimation. This was particularly important because unconscious effects are usually relatively weak. Successful decoding under this procedure indicates that information was sufficiently consistent across participants to support out-of-sample prediction in a held-out individual. Within each training set, we used nested LOPO-CV to select optimal tuning parameters, including the number of PLS components (1–15) and the proportion of voxels retained (0–100% in 25% steps), based on highest prediction accuracy. After parameter optimization, the model was fit to the training data and tested on the left-out participant.

Because the voxel-inclusion threshold was selected within each fold by inner cross-validation, a model could in principle retain no voxels when voxel information did not improve out-of-sample prediction (an intercept-only model). In such folds the prediction reduces to a constant (the training-set mean for continuous targets, or the training-set base rate for binary targets), so the predicted values carry no information about the held-out data. Because a constant predictor yields an undefined or degenerate value for both accuracy metrics used here (Pearson correlation and AUC), these folds were assigned the chance-level accuracy of the corresponding metric (zero for Pearson correlation or 0.50 for AUC).

For binary face decoding, the training data consisted of approximately 2,268 beta maps (28 participants × 3 runs × 27 beta maps) and the test set consisted of 81 beta maps (1 participant × 3 runs × 27 beta maps) per fold. Binary prediction accuracy was quantified using area under the curve (AUC). For continuous SV prediction, the training set comprised approximately 1,008 beta maps (28 participants × 3 runs × 12 beta maps) and the test set

JNeurosci Accepted Manuscript

comprised 36 beta maps (1 participant × 3 runs × 12 beta maps) per fold, with prediction accuracy defined as Pearson's correlation between predicted and observed SV values.

Statistical significance of decoding performance was evaluated using permutation testing. Labels were randomly shuffled within each participant and run, and the analysis was repeated 10,000 times to generate a null distribution. One-tailed p-values were computed by comparing the observed median prediction accuracy to the null distribution. The combined use of AUC metrics and permutation testing ensured that any slight category imbalance (12 face vs. 15 absent trials) did not bias the face decoding results. To generate a null distribution for pair-wise comparisons between seen face vs. absent and unseen face vs. absent decoding accuracies, we applied a sign-flip procedure. On each of the 10,000 permutations, the sign of each participant's accuracy difference was randomly flipped (equivalent to randomly swapping condition labels within participants), and the median of the permuted differences was calculated. This procedure preserved the within-participant dependency structure and yielded a null distribution that reflected the absence of a group difference. The two-sided p-value was calculated as the proportion of permuted statistics with absolute values greater than or equal to the observed statistic.

We also performed cross-decoding to test generalization across conscious awareness (seen and unseen conditions). Using the same LOPO-CV framework, we trained the model on seen face beta maps and tested it on unseen faces in the left-out participant, and vice versa, then averaged prediction accuracy across directions. Importantly, none of the left-out-participant's data was used in the training fold to avoid any statistical dependency between training and testing data. For null distributions, cross-decoding accuracies were likewise averaged across directions before computing permutation-based p-values.

Finally, to generate interpretable T-PLS model coefficients, we built a separate predictor model following the LOPO-CV framework but without nested parameter optimization. This approach allowed us to fit the model to all participants' data and extract voxel-level

JNeurosci Accepted Manuscript

coefficients highlighting predictive patterns for both binary and continuous out-of-sample decoding.

Multivariate control analysis. To determine whether decoding performance was driven by overall activation amplitude or by distributed multivoxel patterns, analyses were repeated under three different feature normalization schemes: mean-only, pattern-only, and pattern-normalized decoding.

In the mean-only analysis, all voxel-wise spatial information within the ROI was removed while preserving the average activation magnitude across voxels for each sample. Specifically, the mean signal across all voxels in the ROI was computed separately for each trial and then replicated across voxels. Decoding performance in this condition therefore reflects information contained solely in the overall univariate activation level of the ROI.

In the pattern-only analysis, the mean activation across voxels within the ROI was removed separately for each trial by subtracting the trial-wise ROI mean from every voxel. This procedure eliminates global shifts in activation level shared across the ROI while preserving the relative spatial distribution of activation across voxels. Decoding performance in this condition therefore reflects information contained in distributed spatial activation patterns beyond the ROI mean signal. However, pattern-only decoding does not fully eliminate all amplitude-related information. Although the global ROI mean is removed, overall pattern amplitude (i.e., the strength or variance of the distributed activation pattern across voxels) can still differ systematically between conditions or subjective value levels and potentially support decoding. To address this issue, a stricter pattern-normalized analysis was additionally performed.

In the pattern-normalized analysis, trial-wise ROI means were first removed as in the pattern-only analysis, after which each trial's multivoxel activation vector was L2-normalized to unit length. This normalization removes differences in overall pattern magnitude, leaving only the relative shape or configuration of activation across voxels. As a result, successful

JNeurosci Accepted Manuscript

decoding in this condition can only be driven by the spatial arrangement of activation values across voxels, rather than by differences in global activation level or distributed activation amplitude.

Together, these analyses allowed us to dissociate decoding based on overall ROI activation amplitude from decoding based on distributed spatial activation patterns, and to test whether decoding effects persisted after controlling for both global and distributed amplitude information.

Results

Behavioral results

Perceptual awareness scale ratings

To confirm that the CFS paradigm worked as intended, we examined the perceptual awareness scale (PAS) responses for the faces in visible, suppressed, and absent conditions. When faces were visibly presented without suppression, they were reported as seen (PAS = 2) on most trials ($Mdn_{proportion}$ = 95.8%, $SE_{proportion}$ = 2.3%, Mdn_{trials} = 69, SE_{trials} = 0.02) with only a few mistakes. When faces were suppressed by CFS, they were reported as unseen (PAS = 1) on most trials ($Mdn_{proportion}$ = 81.3%, $SE_{proportion}$ = 4.2%, Mdn_{trials} = 117, SE_{trials} = 0.04) but sometimes breaking suppression. When faces were absent and an empty background was suppressed with CFS, most trials were reported as unseen (Mdn = 97.8%, SE = 2.6%, Mdn = 44, SE = 0.03), with few false alarms. Overall, the CFS paradigm worked well, awareness reports aligned with expectations and we had enough trials for analysis.

Task performance and reaction times

On trials where the face was “seen” (presented visibly and reported seen), task performance (d’) was much greater than chance (M = 3.39, SE = 0.15, t(28) = 23.04, p < .001, one-tailed; Figure 2). However, when faces were “unseen” (suppressed and reported unseen), task performance was not greater than chance (M = 0.06, SE = 0.07, t(28) = 0.87, p = .19,

JNeurosci Accepted Manuscript

one-tailed). As expected, task performance for seen faces was much greater than for unseen faces ($t(28) = 20.49$, $p < .001$, two-tailed). It was not possible to compute task performance for absent trials since there was no face. There was no direct influence of the unseen faces on task performance, and faces can therefore be considered subliminal by both objective and subjective measures of awareness.

When testing for indirect influences, we examined whether trials with seen and unseen faces differed from trials absent faces, and whether there was a difference between unseen trials when responses were correct (hits & correct rejections) and incorrect (misses & false alarms). Because the face-identification task was easy when the faces were seen, seen incorrect trials were only present in 17 of 29 participants, we therefore did not include them in the ANOVA. The 1 x 4 repeated measures ANOVA revealed a difference ($F(3,28) = 14.76$, $p < .001$) in reaction time across: seen correct ($M_{log(RT)} = 3.06$, $SE = 0.01$), absent ($M_{log(RT)} = 3.11$, $SE = 0.01$), unseen correct ($M_{log(RT)} = 3.12$, $SE = 0.02$), and unseen incorrect ($M_{log(RT)} = 3.13$, $SE = 0.01$).

Post hoc t-tests (Figure 2) revealed that reaction times were faster for seen correct compared to absent ($t(28) = -3.26$, $p_{FDR} = .006$, $p_{unc.} = .003$, two-tailed); unseen correct ($t(28) = -4.09$, $p_{FDR} = .001$, $p_{unc.} < .001$, two-tailed); and unseen incorrect ($t(28) = -4.65$, $p_{FDR} < .001$, $p_{unc.} < .001$, two-tailed). Interestingly, reaction time for unseen correct ($t(28) = -2.58$, $p_{FDR} = .019$, $p_{unc.} = .015$, two-tailed) and unseen incorrect ($t(28) = -3.11$, $p_{FDR} = .006$, $p_{unc.} = .004$, two-tailed) responses were both slower than absent trials. However, there was no difference between unseen correct and incorrect trials ($t(28) = -0.41$, $p_{FDR} = .685$, $p_{unc.} = .685$, two-tailed).

Taken together, these results show that even though unseen and absent faces had the same lack of perceptual awareness and unseen task performance was at chance, the unseen faces slowed reaction time compared to absent trials, suggesting a subliminal memory trace of the unseen faces.

fMRI results

JNeurosci Accepted Manuscript

In the sections below, we first present the univariate results, which test whether the mean neural signal differs between conditions, followed by the multivariate decoding results, which assess whether neural patterns differ between conditions, or in the case of cross-decoding, whether patterns are similar across conditions. For brevity, these results are presented together according to section topic because they are both testing for the presence of face or SV processing. As a reminder, we used the same condition definitions as in the behavioral analyses: “seen” (clearly visible face and reported seen), “unseen” (suppressed face and reported unseen), and “absent” (no face and reported unseen).

Face perception in FFA

To confirm that both seen and unseen faces were processed in higher-level visual areas, we conducted univariate and multivariate ROI analyses in the fusiform face area (FFA; Figure 3).

Seen faces. As expected, seen > absent faces showed significant mean neural signal change ($M = 1.62$, $SE = 0.12$, $t(28) = 13.20$, $p_{FDR} < .001$, $p_{unc.} < .001$, one-tailed), and seen vs. absent out-of-sample decoding showed significant prediction accuracy ($Mdn_{AUC} = 92.8$, $p_{FDR} < .001$, $p_{unc.} < .001$, one-tailed permutation test), with a mix of positive and negative predictor coefficients in the FFA.

Unseen faces. Similarly, unseen > absent faces showed significant neural signal change ($M = 0.10$, $SE = 0.06$, $t(28) = 1.76$, $p_{FDR} = .045$, $p_{unc.} = .045$, one-tailed), and unseen vs. absent decoding showed a significant prediction accuracy ($Mdn_{AUC} = 54.6$, $p_{FDR} = .006$, $p_{unc.} = .005$, one-tailed permutation test), with a mix of positive and negative predictor coefficients in the FFA.

Cross-decoding. Presence vs. absence could be cross-decoded across seen and unseen faces in the FFA ($Mdn_{AUC} = 62.0$, $p_{FDR} = .002$, $p_{unc.} < .001$, one-tailed permutation test). Taken together, these findings suggest that both seen and unseen faces were processed in the FFA with a shared neural code.

JNeurosci Accepted Manuscript

Seen and unseen comparisons. The neural difference for seen > absent faces were significantly greater than unseen > absent faces ($t(28) = 13.79$, $p_{FDR} < .001$, $p_{unc.} < .001$, two-tailed), and the decoding accuracy for seen vs. absent faces was significantly greater than unseen vs. absent faces ($p_{FDR} < .001$, $p_{unc.} < .001$, two-tailed permutation test). These results show that seen faces produced a much stronger neural response in the FFA than unseen faces.

Control analyses. To determine contributions from global activation and distributed multivoxel patterns on decoding performance, decoding was separately tested using mean-only, pattern-only, and pattern-normalized signals. These analyses isolated information carried by overall ROI activation, distributed spatial patterns, and pattern shape independent of activation amplitude, respectively.

For seen faces, decoding in FFA was robust across all signal components (mean-only, $Mdn_{AUC} = 87.1$, $p_{unc.} < .001$; pattern-only, $Mdn_{AUC} = 92.8$, $p_{unc.} < .001$; pattern-normalized, $Mdn_{AUC} = 91.6$, $p_{unc.} < .001$, one-tailed permutation test). In contrast, unseen face decoding was at chance in the mean-only condition ($Mdn_{AUC} = 50.0$, $p_{unc.} = .928$, one-tailed permutation test), but remained significantly above chance when multivoxel pattern information was preserved (pattern-only, $Mdn_{AUC} = 54.8$, $p_{unc.} < .001$; pattern-normalized, $Mdn_{AUC} = 62.7$, $p_{unc.} < .001$, one-tailed permutation test). Cross-decoding between seen and unseen faces was significant across all analyses (mean-only, $Mdn_{AUC} = 53.0$, $p_{unc.} = .006$; pattern, $Mdn_{AUC} = 66.5$, $p_{unc.} < .001$; pattern-normalized, $Mdn_{AUC} = 67.2$, $p_{unc.} < .001$, one-tailed permutation tests).

Overall, unseen face decoding depended primarily on distributed multivoxel pattern information rather than mean activation differences, and remained significant after controlling for both global activation and overall pattern amplitude.

Subjective value in aVS and vmPFC

To test whether subjective value (SV; operationalized as the idiosyncratic continuous measure of overall facial attractiveness) can be automatically computed in the aVS and

JNeurosci Accepted Manuscript

vmPFC independently of conscious awareness, we tested for a positive relationship between SV ratings and neural signal for both seen and unseen faces with univariate parametric modulations and multivariate regression predictions (Figure 4).

Seen faces. In the vmPFC, SV ratings were positively related to mean neural signal (M = 0.14, SE = 0.06, t(28) = 2.26, p_{FDR} = .036, $p_{unc.}$ = .016, one-tailed), and multivariate regression with continuous SV ratings achieved significant out-of-sample prediction accuracy (Mdn_r = 0.091, p_{FDR} = .048, $p_{unc.}$ = .029, one-tailed permutation test), with positive predictor coefficients. In the aVS, however, no significant relationship was observed for mean BOLD signal (M = 0.01, SE = 0.02, t(28) = 0.57 p_{FDR} = .320, $p_{unc.}$ = .288, one-tailed) and prediction accuracy was non-significant (Mdn_r = 0, p_{FDR} = .822, $p_{unc.}$ = .822, one-tailed permutation test).

Unseen faces. In the vmPFC, SV ratings were again positively related to mean neural signal (M = 0.14, SE = 0.06, t(28) = 2.21, p_{FDR} = .036, $p_{unc.}$ = .018, one-tailed; Wilcoxon signed rank test to account for an outlier, Z = 2.00, p_{FDR} = .045, $p_{unc.}$ = .023, one-tailed), and multivariate regression produced significant prediction accuracy (Mdn_r = 0.086, p_{FDR} = .049, $p_{unc.}$ = .034, one-tailed permutation test) with positive predictor coefficients. In the aVS, SV ratings showed a significant positive relationship with mean neural signal (M = 0.05, SE = 0.02, t(28) = 2.80, p_{FDR} = .017, $p_{unc.}$ = .005, one-tailed), and multivariate regression significantly predicted SV (Mdn_r = 0.136, p_{FDR} = .010, $p_{unc.}$ = .002, one-tailed permutation test), with mostly positive predictor coefficients.

Cross-decoding. SV could be cross-decoded across seen and unseen faces in the vmPFC (Mdn_r = 0.069, p_{FDR} = .010, $p_{unc.}$ = .001, one-tailed permutation test), but not in the aVS (Mdn_r = 0.015, p_{FDR} = .151, $p_{unc.}$ = .121, one-tailed permutation test).

Seen and unseen face comparisons. In the vmPFC, the neural relationship with SV did not significantly differ in strength between seen and unseen faces with univariate (t(28) = 0.05, p_{FDR} = .999, $p_{unc.}$ = .962, two-tailed) or multivariate analysis (p_{FDR} > .999, $p_{unc.}$ > .999, two-tailed permutation test). In the aVS, the neural relationship with SV was significantly stronger for

JNeurosci Accepted Manuscript

unseen than seen faces with multivariate (p_{FDR} = .012, $p_{unc.}$ = .003, two-tailed permutation test) but not with univariate analysis (t(28) = 1.22, p_{FDR} = .468, $p_{unc.}$ = .234, two-tailed). The results show that SV was processed at a similar strength in vmPFC when faces were seen and unseen, but at a greater strength in aVS when faces were unseen compared to seen, likely due to the lack of a significant neural SV-signal in aVS for seen faces.

Control analyses. To isolate contributions of global activation and distributed multivoxel patterns, decoding analyses were repeated using mean-only, pattern-only, and pattern-normalized signals. For seen trials, SV decoding was inconsistent across ROIs and signal components. In vmPFC, decoding was significant only in the mean-only condition (Mdn_r = 0.11, p_{unc} = .005, one-tailed permutation test), but not for pattern-only or pattern-normalized signals (both ps_{unc} > .90), suggesting that the full-model decoding was mainly driven by mean activation amplitude. In aVS, decoding was not above chance for any signal component (both ps_{unc} > .865).

For unseen trials, a similar pattern was observed. In vmPFC, decoding did not reach significance in any condition (mean-only, Mdn_r = 0.059, p_{unc} = .056; pattern-only, Mdn_r = 0.050, p_{unc} = .073; pattern-normalized, Mdn_r = 0.000, p_{unc} = .764; one-tailed permutation test), but suggest that the full-model decoding effect was driven by the combined effect of mean activation and distributed amplitude differences. In contrast, aVS showed significant decoding only for the mean-only signal (Mdn_r = 0.11, p_{unc} = .005, one-tailed permutation test), but not for pattern or pattern-normalized signals (both ps_{unc} > .142).

Cross-decoding between seen and unseen trials also differed across ROIs. In vmPFC, cross-decoding was significant across all signal components (mean-only, Mdn_r = 0.065, p_{unc} = .005; pattern-only, Mdn_r = 0.060, p_{unc} = .003; pattern-normalized signals, Mdn_r = 0.013, p_{unc} = .045; one-tailed permutation test). In aVS, cross-decoding was significant only in the mean-only condition (Mdn_r = 0.021, p_{unc} = .038), but not in the pattern or pattern-normalized conditions (both ps_{unc} > .678). Follow-up directional analyses indicated that the aVS cross-decoding effect was driven primarily by unseen-to-seen generalization (mean-only, Mdn_r =

JNeurosci Accepted Manuscript

543 0.041, p_{unc} = .0179), whereas seen-to-unseen decoding was at chance (mean-only, Mdn_r =
544 0.000, p_{unc} = .886), suggesting that seen aVS responses contained weak but reliable SV-
545 related information that was not able to achieve significant within-condition decoding.

546 Together, these results show that SV is computed in vmPFC for both seen and unseen
547 faces, with similar strength and representation across seen and unseen faces. In contrast,
548 decoding was only successful in aVS for unseen faces. Control analyses suggest that SV
549 decoding is largely driven by univariate signals, and detected weak SV signals in aVS for seen
550 faces when using a model trained on SV patterns of unseen faces.

551 *Relationship between face perception in FFA and SV in aVS and vmPFC*

552 We also examined whether face-signal strength in the FFA was related to SV-signal
553 strength in the aVS and vmPFC (Figure 5). For unseen faces, Spearman rank correlations
554 between FFA contrast estimates (unseen > absent) and SV-related parametric contrast
555 estimates showed positive relationships with both aVS (r(27) = 0.43, p_{FDR} = .019, $p_{unc.}$ = .001,
556 one-tailed) and vmPFC (r(27) = 0.57, p_{FDR} = .003, $p_{unc.}$ < .001, one-tailed). For seen faces,
557 however, no significant relationships were found with aVS (r(27) = 0.19, p_{FDR} = .217, $p_{unc.}$ =
558 .163, one-tailed) or vmPFC (r(27) = -0.08, p_{FDR} = .669, $p_{unc.}$ = .669, one-tailed). These findings
559 suggest that stronger unseen face processing in the FFA is associated with stronger SV
560 processing in both aVS and vmPFC.

561 *Relationship between neural SV signals and behavior*

562 There was no significant relationships between SV processing of seen faces in aVS
563 (r(27) = 0.20, p_{FDR} = .766, $p_{unc.}$ = .304, two-tailed) or vmPFC (r(27) = -0.06, p_{FDR} = . 766, $p_{unc.}$
564 = .766, two-tailed) and reaction time. Similarly, we did not find any significant relationship
565 between SV processing from unseen faces in aVS (r(27) = 0.09, p_{FDR} = . 766, $p_{unc.}$ = .660, two-
566 tailed) or vmPFC (r(27) = 0.07, p_{FDR} = . 766, $p_{unc.}$ = .701, two-tailed) and reaction time.

567 *Whole-brain results*

JNeurosci Accepted Manuscript

TFCE-adjusted and FDR corrected whole-brain contrasts were used to explore whether there was neural signal in any brain areas outside of our ROIs that was associated with seen or unseen face perception and seen or unseen SV processing (Figure 6).

Seen faces. The linear parametric SV modulation of seen faces revealed several clusters where neural signal had a positive relationship to SV, including bilaterally in the anterior cingulate cortex and extending through the dorsomedial prefrontal cortex (dmPFC), the cerebellum, the middle frontal gyrus, and precentral gyrus (Figure 6A). The contrast for seen > absent faces revealed significant neural signal in the bilateral vmPFC and right aVS, together with many other brain areas, including bilateral dorsal posterior cingulate cortex (dPPC), precuneus, and large bilateral areas of the temporal cortex (including FFA), parietal cortex, frontal cortex, cerebellum, and subcortical areas such as putamen, amygdala, and hippocampus (Figure 6B).

Seen and unseen face comparisons. When comparing the parametric contrasts for seen > unseen SV, no differences survived FDR corrections. However, the contrast for seen > unseen faces did reveal significant differences. Specifically, seen faces were associated with a greater neural signal in the right aVS and several other brain areas, including bilateral dPPC, precuneus, and large bilateral areas of the temporal cortex (including FFA), parietal cortex, frontal cortex, cerebellum, and subcortical areas such as putamen, amygdala, and hippocampus (Figure 6C). Instead, unseen faces were associated with a greater neural signal in areas such as the bilateral occipital cortex, supramarginal gyrus, inferior frontal gyrus and precentral gyrus, ventral posterior cingulate cortex (vPPC), precuneus, insula, and subcortical areas such as caudate nucleus (extending slightly into left aVS) and thalamus (Figure 6C).

Relationship between neural SV signal and behavior. Neither whole brain correlations between seen reaction times and neural SV signals from seen faces, or between unseen reaction times and neural SV signals from unseen faces, survived whole-brain FDR corrections.

JNeurosci Accepted Manuscript

Discussion

We tested whether SV (operationalized as facial attractiveness) can be processed automatically in aVS and vmPFC without conscious awareness. We found that (i) subliminal faces elicited SV responses in both aVS and vmPFC, with vmPFC additionally showing similar neural SV response for conscious and subliminal faces; (ii) subliminal faces were processed in FFA with a similar but weaker neural representation as conscious faces; and (iii) stronger subliminal FFA processing was associated with stronger subliminal SV processing in aVS and vmPFC. These results suggest that SV can be computed automatically, in a bottom-up fashion, in core valuation circuits outside conscious awareness.

Our findings extend previous work on automatic SV computation by addressing limitations in earlier studies. Previous studies showed that aVS and vmPFC encode SV during passive viewing or unrelated tasks (Kim et al., 2007; Lebreton et al., 2009; Levy et al., 2011; Smith et al., 2014; Tusche et al., 2010), but spontaneous explicit evaluations are difficult to rule out when stimuli are consciously presented. Subliminal presentations remove this confound, but previous attempts were limited in several ways (Bijleveld et al., 2014; Fernandes et al., 2025; Gillath & Canterberry, 2012; Ito et al., 2015; Oei et al., 2012; Pessiglione et al., 2007, 2008): (i) trial-wise awareness measures were not used, so conscious trials may have been included; (ii) SV was not measured with idiosyncratic participant-specific ratings; (iii) subliminal information was often task-relevant, leaving top-down influences possible; and/or (iv) no SV effects were found in the brain's valuation areas (aVS and vmPFC). We addressed these issues by combining CFS with trial-wise objective and subjective awareness measures during fMRI, and linked signal in core valuation areas to participant-specific continuous post-fMRI SV ratings. Our results therefore provide the strongest evidence to date that core valuation circuits, including vmPFC, automatically compute SV without conscious awareness, demonstrated here for the first time with facial attractiveness.

JNeurosci Accepted Manuscript

That subliminal SV processing extended from aVS to vmPFC is consistent with our other work showing that subliminal probabilities can be processed within these same regions (Fernandes et al., 2025). Together, these two studies, using different stimuli and tasks, make a strong case that SV computations in vmPFC operate outside conscious awareness. This supports the idea that facial attractiveness engages the same domain-general "common currency" circuitry as other value domains, plausibly because attractiveness reflects the desirability of a potential mate (Buss, 1989; Buss & Schmitt, 2019). Univariate studies and meta-analyses show overlapping aVS and vmPFC signals for faces and other rewards (Bartra et al., 2013; Chuan-Peng et al., 2020; Kim et al., 2007; Lebreton et al., 2009), and by findings that neural representations of attractiveness generalize across stimulus categories (Pegors et al., 2015). Consistent with a causal role for this circuitry, vmPFC anatomy and vmPFC lesions are associated with individual differences and disruptions of choice preferences (Bergström, Lerman, et al., 2024; Bergström, Schu, et al., 2024; Camille et al., 2011; Fellows & Farah, 2007; Godefroy et al., 2024; Yu et al., 2022). Our results therefore challenge the assumption that subliminal SV processing is confined to rudimentary subcortical mechanisms (Bijleveld et al., 2012), while adding to reports of subliminal value processing in subcortical regions (Fernandes et al., 2025; Oei et al., 2012; Pessiglione et al., 2007, 2008). However, here and previously the subliminal stimuli represented one-dimensional SV (e.g., attractiveness, probability, or monetary reward). Whether SV can be computed subliminally from multi-attribute stimuli, or several attributes integrated without conscious awareness, remains open.

Our results contrast with the only other fMRI study of subliminal facial attractiveness, which found aVS and vmPFC effects only for consciously seen faces (Ito et al., 2015). Methodological differences likely explain this discrepancy: their brief backward-masked presentations (34 ms) may have produced weaker subliminal effects than our three-second CFS presentations, and their ROI definition may have missed the vmPFC subregion most reliably associated with SV and facial attractiveness (Bartra et al., 2013; Chuan-Peng et al., 2020). Instead, subliminal attractiveness effects have been reported outside valuation circuits:

JNeurosci Accepted Manuscript

marginal effects in dmPFC and ventrolateral prefrontal cortex/anterior insula (Ito et al., 2015), and posterior visual/parietal areas in EEG (Hou et al., 2023; Shang et al., 2025). These regions are commonly associated with salience, the capacity of a stimulus to capture attention or increase arousal, than with SV.

Salience has a U-shaped relationship with SV but correlates with SV when negative values are absent, and is typically associated with signal in anterior insula, caudate nucleus, dmPFC, dorsolateral prefrontal cortex, and inferior posterior parietal cortex (Bartra et al., 2013; Kahnt et al., 2014; Kahnt & Tobler, 2017; Litt et al., 2011; Zink et al., 2004). While our design cannot dissociate SV from salience, because our stimuli lacked negatively rated faces, prior work shows that when these factors are dissociated, aVS and vmPFC signals reflect SV but not salience (Bartra et al., 2013; Fernandes et al., 2025; Kahnt et al., 2014; Litt et al., 2011). Our whole-brain association between dmPFC signal for seen faces and SV ratings may therefore reflect salience rather than SV.

A related question concerns the format in which value is encoded rather than its anatomical locus. Most models assume SV is a scalar quantity reflected in response amplitude. Although multivariate decoding showed similar value representations across Seen and Unseen conditions, this does not imply a spatially distributed code beyond a scalar one. Our control analyses suggest SV was encoded primarily in amplitude rather than patterned information. The multivariate analyses are therefore best understood as exploiting univariate effects, functioning as a data-driven weighted ROI analysis, rather than identifying a distinct representational format. Interestingly, the reverse held for unseen face representations, which appear driven mainly by distributed patterns rather than overall amplitude.

We replicate earlier findings of subliminal face processing in the FFA (e.g., Fang & He, 2005; Jiang & He, 2006; Moutoussis & Zeki, 2002), and additionally found that stronger subliminal FFA responses correlated with stronger SV responses in aVS and vmPFC. FFA is specialized for invariant facial structure used in identification (George et al., 1999; Hoffman & Haxby, 2000; Kanwisher et al., 1997) and likely provides the structural facial information on

JNeurosci Accepted Manuscript

673 which attractiveness judgments rely, such as symmetry, averageness, and sexual dimorphism
674 (Rhodes, 2006). This interpretation is consistent with evidence from effective connectivity from
675 FFA to vmPFC (Fairhall & Ishai, 2007) and with impaired attractiveness judgments in
676 prosopagnosia patients with FFA lesions (Iaria et al., 2008). The absence of this correlation
677 for seen faces may indicate that the relationship is more apparent when processing is strongly
678 suppressed, with suppression strength varying across individuals.

679 We observed relatively weak vmPFC effects for seen faces despite robust neural
680 responses to the faces themselves, and no reliable SV effects in aVS for seen faces, although
681 the unseen-to-seen cross-decoding control analysis suggests a weak aVS SV signal. Several
682 factors may contribute. First, our paradigm probed implicit rather than explicit valuation: robust
683 SV signals in aVS and vmPFC are typically observed when participants consciously evaluate
684 stimulus value, whereas value signals elicited without explicit evaluation may be weaker and
685 less consistent. Second, the seen condition contained substantially fewer trials, because the
686 design deliberately prioritized the suppressed condition to maximize sensitivity for detecting
687 subliminal value information, further reducing power. Third, because most trials contained
688 suppressed or absent faces, visible faces occurred infrequently, and their sudden appearance
689 may have elicited surprise, arousal, or motivational signals related to anticipating successful
690 task performance that masked value-related activity. Consistent with this, intrinsic reward
691 prediction error signals in aVS occur during successful memory performance even without
692 explicit feedback or rewards (Satterthwaite et al., 2012; Wolf et al., 2011). Finally, participants
693 could actively engage with visible faces during the memory task, whereas suppressed faces
694 were necessarily processed more passively, and differences in engagement and attentional
695 allocation may have introduced additional variance in the visible condition.

696 Although subliminal faces did not directly influence task performance, participants
697 responded more slowly to subliminal than absent trials, suggesting a lingering memory trace,
698 consistent with similar memory paradigms (Bergström & Eriksson, 2014, 2015, 2018; Franco-

JNeurosci Accepted Manuscript

Martínez et al., 2026; Pedale et al., 2023). SV processing in aVS or vmPFC did not appear to influence reaction time, perhaps because the face-identification task was unrelated to SV.

A continuing debate concerns how best to measure the absence of conscious awareness. We used both subjective (PAS) and objective (face identity) trial-wise measures, the recommended approach in the field (Stockart et al., 2025), with a two-button PAS sufficient to distinguish "no experience" from "vague visual experience" (Fernandes et al., 2025). Suppressed faces and absent trials were consistently rated as "no experience," and objective performance was at chance for unseen faces. The observed reaction time, neural face, and neural SV effects from unseen faces when both measures indicated unawareness therefore strongly supports that these effects were truly subliminal.

In conclusion, SV (operationalized as facial attractiveness) can be automatically processed in aVS and vmPFC without conscious awareness. These results suggest an avenue for automatic subliminal influences on value-based decisions. Whether conscious awareness is necessary for later stages of the decision process remains for future research.

Author Contributions

FB: Conceptualization, funding acquisition, supervision, project administration, methodology, investigation, formal analysis, visualization, validation, data curation, writing – original draft, writing – review & editing. PF: Software, Investigation, formal analysis, writing – review & editing. JWK: Methodology and writing – review & editing. AT: Methodology and writing – review & editing. JA: Methodology and writing – review & editing. CR: Methodology and writing – review & editing.

Declaration of Competing Interest

The authors declare no competing interests.

Data availability statement

JNeurosci Accepted Manuscript

The data supporting this study is stored at The Open Science Framework and will be publicly available after the completion of ongoing and future research, or from the corresponding author upon reasonable request.

Code availability statement

The Matlab code for the SHINE Toolbox can be found at Github (https://github.com/RodDalBen/SHINE_color). The custom Matlab code used to create the CFS stimuli can be found at Martin Hebart's webpage (http://martin-hebart.de/webpages/code/stimuli.html). The Thresholded Partial Least Squares (T-PLS) toolbox used for the multivariate decoding analyses can be found at Github (https://github.com/sangillee/TPLSm).

Funding/Acknowledgements

This work was supported by The BIAL Foundation (Grant # 315/20) to FB. FB was supported by Fundação para a Ciência e Tecnologia (CEECIND/03661/2017). JA was supported by a European Research Counsil (ERC) under the European Union's Horizon 2020 research and innovation program Starting Grant number 802553 "Content Map", and by European Research Executive Agency Widening program under the European Union's Horizon Europe Grant 101087584 "Cogbooster".

References

Almeida, J., Fracasso, A., Kristensen, S., Valério, D., Bergström, F., Chakravarthi, R., Tal, Z., & Walbrin, J. (2023). Neural and behavioral signatures of the multidimensionality of manipulable object processing. *Communications Biology*, *6*(1), 1–15. https://doi.org/10.1038/s42003-023-05323-x

Bartra, O., McGuire, J. T., & Kable, J. W. (2013). The valuation system: A coordinate-based meta-analysis of BOLD fMRI experiments examining neural correlates of subjective value. *NeuroImage*, *76*, 412–427. https://doi.org/10.1016/j.neuroimage.2013.02.063

Bergström, F., & Eriksson, J. (2014). Maintenance of non-consciously presented information engages the prefrontal cortex. *Frontiers in Human Neuroscience*, *8*(938), 1–10. https://doi.org/10.3389/fnhum.2014.00938

JNeurosci Accepted Manuscript

751 Bergström, F., & Eriksson, J. (2015). The conjunction of non-consciously perceived object
752 identity and spatial position can be retained during a visual short-term memory task.
753 *Frontiers in Psychology*, *6*(1460), 1–9. https://doi.org/10.3389/fpsyg.2015.01470

754 Bergström, F., & Eriksson, J. (2018). Neural evidence for non-conscious working memory.
755 *Cerebral Cortex*, *28*(9), 3217–3228. https://doi.org/10.1093/cercor/bhx193

756 Bergström, F., Lerman, C., & Kable, J. W. (2024). Reduced cortical complexity in
757 ventromedial prefrontal cortex is associated with a greater preference for risky and
758 immediate rewards. *Imaging Neuroscience*, *2*, 1–14.
759 https://doi.org/10.1162/imag_a_00143

760 Bergström, F., Schu, G., Lee, S., Lerman, C., & Kable, J. W. (2024). Multivariate analysis of
761 multimodal brain structure predicts individual differences in risk and intertemporal
762 preference. *BioRxiv*, 1–31. https://doi.org/https://doi.org/10.1101/2024.07.04.602046

763 Bergström, F., Wurm, M., Valério, D., Lingnau, A., & Almeida, J. (2021). Decoding stimuli
764 (tool-hand) and viewpoint invariant grasp-type information. *Cortex*, *139*, 152–165.
765 https://doi.org/10.1016/j.cortex.2021.03.004

766 Bijleveld, E., Custers, R., & Aarts, H. (2012). Human Reward Pursuit: From Rudimentary to
767 Higher-Level Functions. *Current Directions in Psychological Science*, *21*(3), 194–199.
768 https://doi.org/10.1177/0963721412438463

769 Bijleveld, E., Custers, R., Van der Stigchel, S., Aarts, H., Pas, P., & Vink, M. (2014). Distinct
770 neural responses to conscious versus unconscious monetary reward cues. *Human*
771 *Brain Mapping*, *35*(11), 5578–5586. https://doi.org/10.1002/hbm.22571

772 Buss, D. M. (1989). Sex differences in human mate preferences: Evolutionary hypotheses
773 tested in 37 cultures. *Behavioral and Brain Sciences*, *12*(1), 1–14.
774 https://doi.org/10.1017/S0140525X00023992

775 Buss, D. M., & Schmitt, D. P. (2019). Mate Preferences and Their Behavioral Manifestations.
776 *Annual Review of Psychology*, *70*, 77–110. https://doi.org/10.1146/annurev-psych-
777 010418-103408

778 Camille, N., Griffiths, C. A., Vo, K., Fellows, L. K., & Kable, J. W. (2011). Ventromedial
779 frontal lobe damage disrupts value maximization in humans. *Journal of Neuroscience*,
780 *31*(20), 7527–7532. https://doi.org/10.1523/JNEUROSCI.6527-10.2011

781 Chib, V. S., Rangel, A., Shimojo, S., & O'Doherty, J. P. (2009). Evidence for a common
782 representation of decision values for dissimilar goods in human ventromedial prefrontal
783 cortex. *Journal of Neuroscience*, *29*(39), 12315–12320.
784 https://doi.org/10.1523/JNEUROSCI.2575-09.2009

785 Chuan-Peng, H., Huang, Y., Eickhoff, S. B., Peng, K., & Sui, J. (2020). Seeking the "Beauty
786 Center" in the Brain: A Meta-Analysis of fMRI Studies of Beautiful Human Faces and
787 Visual Art. *Cognitive, Affective and Behavioral Neuroscience*, *20*(6), 1200–1215.
788 https://doi.org/10.3758/s13415-020-00827-z

789 Dal Ben, R. (2023). SHINE_color: Controlling low-level properties of colorful images.
790 *MethodsX*, *11*(3), 102377. https://doi.org/10.1016/j.mex.2023.102377

791 Engell, A. D., Haxby, J. V., & Todorov, A. (2007). Implicit trustworthiness decisions:
792 Automatic coding of face properties in the human amygdala. *Journal of Cognitive*
793 *Neuroscience*, *19*(9), 1508–1519. https://doi.org/10.1162/jocn.2007.19.9.1508

JNeurosci Accepted Manuscript

Fairhall, S. L., & Ishai, A. (2007). Effective connectivity within the distributed cortical network for face perception. *Cerebral Cortex*, *17*(10), 2400–2406. https://doi.org/10.1093/cercor/bhl148

Fang, F., & He, S. (2005). Cortical responses to invisible objects in the human dorsal and ventral pathways. *Nature Neuroscience*, *8*(10), 1380–1385. https://doi.org/10.1038/nn1537

Fellows, L. K., & Farah, M. J. (2007). The role of ventromedial prefrontal cortex in decision making: Judgment under uncertainty or judgment per se? *Cerebral Cortex*, *17*(11), 2669–2674. https://doi.org/10.1093/cercor/bhl176

Fernandes, P., Lee, S., Kable, J. W., Seidel, P., Almeida, J., Eriksson, J., de Sousa, B., & Bergström, F. (2025). Subliminal risk influences subjective value in the ventromedial prefrontal cortex. In *BioRxiv*. https://doi.org/10.1101/2025.03.11.642695

Fontan, A., Lindgren, L., Pedale, T., Brorsson, C., Bergström, F., & Eriksson, J. (2021). A reduced level of consciousness affects non-conscious processes. *NeuroImage*, *244*(April), 118571. https://doi.org/10.1016/j.neuroimage.2021.118571

Franco-Martínez, A., Rey-Sáez, R., Adrián-Ventura, J., Amerio, P., Baciero, A., Bennis, A., Bergström, F., Cleeremans, A., Contu, L., Dell'Acqua, R., Deng, X., Dolu, F. N., Gambarota, F., Gao, Y., Garre-Frutos, F., Grubert, A., Hernando, A., Hinojosa, J. A., Hoory, A., … Vadillo, M. A. (2026). Replicating the unconscious working memory effect: a multisite Registered Report. *Neuroscience of Consciousness*, *2026*(1). https://doi.org/10.1093/nc/niaf046

George N, Dolan R, Fink G, Baylis G, Russell C, & Driver J. (1999). Contrast polarity and face recognition in the human fusiform gyrus. *Nature Neuroscience*, *2*(6), 574–580.

Gillath, O., & Canterberry, M. (2012). Neural correlates of exposure to subliminal and supraliminal sexual cues. *Social Cognitive and Affective Neuroscience*, *7*(8), 924–936. https://doi.org/10.1093/scan/nsr065

Godefroy, V., Durand, A., Simon, M., Weber, B., Kable, J., Lerman, C., Bergström, F., Levy, R., Batrancourt, B., Schmidt, L., Plassmann, H., & Koban, L. (2024). *A structural MRI marker predicts individual differences in impulsivity and classifies patients with behavioral-variant frontotemporal dementia from matched controls* (Vol. 2, Number 8). https://doi.org/10.1101/2024.09.12.612706

Grill-Spector, K., Weiner, K. S., Kay, K., & Gomez, J. (2017). The Functional Neuroanatomy of Human Face Perception. *Annual Review of Vision Science*, *3*, 167–196. https://doi.org/10.1146/annurev-vision-102016-061214

Grueschow, M., Polania, R., Hare, T. A., & Ruff, C. C. (2015). Automatic versus Choice-Dependent Value Representations in the Human Brain. *Neuron*, *85*(4), 874–885. https://doi.org/10.1016/j.neuron.2014.12.054

Hoffman, E. A., & Haxby, J. V. (2000). Distinct representations of eye gaze and identity in the distributed human neural system for face perception. *Nature Neuroscience*, *3*(1), 80–84. https://doi.org/10.1038/71152

Hou, X., Shang, J., & Tong, S. (2023). Neural Mechanisms of the Conscious and Subliminal Processing of Facial Attractiveness. *Brain Sciences*, *13*(6), 855. https://doi.org/10.3390/brainsci13060855

JNeurosci Accepted Manuscript

Iaria, G., Fox, C. J., Waite, C. T., Aharon, I., & Barton, J. J. S. (2008). The contribution of the fusiform gyrus and superior temporal sulcus in processing facial attractiveness: Neuropsychological and neuroimaging evidence. *Neuroscience*, *155*(2), 409–422. https://doi.org/10.1016/j.neuroscience.2008.05.046

Ito, A., Abe, N., Kawachi, Y., Kawasaki, I., Ueno, A., Yoshida, K., Sakai, S., Matsue, Y., & Fujii, T. (2015). Distinct neural correlates of the preference-related valuation of supraliminally and subliminally presented faces. *Human Brain Mapping*, *36*(8), 2865–2877. https://doi.org/10.1002/hbm.22813

Jiang, Y., & He, S. (2006). Cortical Responses to Invisible Faces: Dissociating Subsystems for Facial-Information Processing. *Current Biology*, *16*(20), 2023–2029. https://doi.org/10.1016/j.cub.2006.08.084

Kable, J. W., & Glimcher, P. W. (2007). The neural correlates of subjective value during intertemporal choice. *Nature Neuroscience*, *10*(12), 1625–1633. https://doi.org/10.1038/nn2007

Kable, J. W., & Glimcher, P. W. (2009). The Neurobiology of Decision: Consensus and Controversy. *Neuron*, *63*(6), 733–745. https://doi.org/10.1016/j.neuron.2009.09.003

Kahnt, T., Park, S. Q., Haynes, J.-D., & Tobler, P. N. (2014). Disentangling neural representations of value and salience in the human brain. *Proceedings of the National Academy of Sciences*, *111*(13), 5000–5005. https://doi.org/10.1073/pnas.1320189111

Kahnt, T., & Tobler, P. N. (2017). Reward, Value, and Salience. In *Decision Neuroscience* (pp. 109–120). Elsevier. https://doi.org/10.1016/B978-0-12-805308-9.00009-9

Kanwisher, N., McDermott, J., & Chun, M. M. (1997). The fusiform face area: a module in human extrastriate cortex specialized for face perception. *The Journal of Neuroscience : The Official Journal of the Society for Neuroscience*, *17*(11), 4302–4311. https://doi.org/10.1098/Rstb.2006.1934

Kim, H., Adolphs, R., O'Doherty, J. P., & Shimojo, S. (2007). Temporal isolation of neural processes underlying face preference decisions. *Proceedings of the National Academy of Sciences*, *104*(46), 18253–18258. https://doi.org/10.1073/pnas.0703101104

Lebreton, M., Jorge, S., Michel, V., Thirion, B., & Pessiglione, M. (2009). An Automatic Valuation System in the Human Brain: Evidence from Functional Neuroimaging. *Neuron*, *64*(3), 431–439. https://doi.org/10.1016/j.neuron.2009.09.040

Lee, S., Bradlow, E. T., & Kable, J. W. (2022). Fast construction of interpretable whole-brain decoders. *Cell Reports Methods*, *2*(6), 100227. https://doi.org/10.1016/j.crmeth.2022.100227

Levy, D. J., & Glimcher, P. W. (2012). The root of all value: A neural common currency for choice. *Current Opinion in Neurobiology*, *22*(6), 1027–1038. https://doi.org/10.1016/j.conb.2012.06.001

Levy, I., Lazzaro, S. C., Rutledge, R. B., & Glimcher, P. W. (2011). Choice from non-choice: Predicting consumer preferences from blood oxygenation level-dependent signals obtained during passive viewing. *Journal of Neuroscience*, *31*(1), 118–125. https://doi.org/10.1523/JNEUROSCI.3214-10.2011

JNeurosci Accepted Manuscript

878 Litt, A., Plassmann, H., Shiv, B., & Rangel, A. (2011). Dissociating valuation and saliency
879 signals during decision-making. *Cerebral Cortex*, *21*(1), 95–102.
880 https://doi.org/10.1093/cercor/bhq065

881 Ma, D. S., Correll, J., & Wittenbrink, B. (2015). The Chicago face database: A free stimulus
882 set of faces and norming data. *Behavior Research Methods*, *47*(4), 1122–1135.
883 https://doi.org/10.3758/s13428-014-0532-5

884 Miao, C., Li, X., Derrington, E., Moisan, F., Li, Y., & Dreher, J. C. (2022). ERPs responses to
885 dominance features from human faces. *Scientific Reports*, *12*(1), 1–9.
886 https://doi.org/10.1038/s41598-022-25370-4

887 Moutoussis, K., & Zeki, S. (2002). The relationship between cortical activation and
888 perception investigated with invisible stimuli. *Proceedings of the National Academy of*
889 *Sciences of the United States of America*, *99*(14), 9527–9532.
890 https://doi.org/10.1073/pnas.142305699

891 Newell, B. R., & Shanks, D. R. (2014). Unconscious influences on decision making: A critical
892 review. *Behavioral and Brain Sciences*, *37*(1), 1–19.
893 https://doi.org/10.1017/S0140525X12003214

894 Oei, N. Y. L., Rombouts, S. A., Soeter, R. P., Van Gerven, J. M., & Both, S. (2012).
895 Dopamine modulates reward system activity during subconscious processing of sexual
896 stimuli. *Neuropsychopharmacology*, *37*(7), 1729–1737.
897 https://doi.org/10.1038/npp.2012.19

898 Pedale, T., Fontan, A., Grill, F., Bergström, F., & Eriksson, J. (2023). Nonconscious
899 information can be identified as task-relevant but not prioritized in working memory.
900 *Cerebral Cortex*, 1–15. https://doi.org/10.1093/cercor/bhac208

901 Pegors, T. K., Kable, J. W., Chatterjee, A., & Epstein, R. A. (2015). Common and Unique
902 Representations in pFC for Face and Place Attractiveness. *Journal of Cognitive*
903 *Neuroscience*, *27*(5), 959–973. https://doi.org/10.1162/jocn_a_00777

904 Pessiglione, M., Petrovic, P., Daunizeau, J., Palminteri, S., Dolan, R. J., & Frith, C. D.
905 (2008). Subliminal Instrumental Conditioning Demonstrated in the Human Brain.
906 *Neuron*, *59*(4), 561–567. https://doi.org/10.1016/j.neuron.2008.07.005

907 Pessiglione, M., Schmidt, L., Draganski, B., Kalisch, R., Lau, H., Dolan, R. J., & Frith, C. D.
908 (2007). How the brain translates money into force: a neuroimaging study of subliminal
909 motivation. *Science (New York, N.Y.)*, *316*(5826), 904–906.
910 https://doi.org/10.1126/science.1140459

911 Ratcliff, R. (1993). Methods for dealing with reaction time outliers. *Psychological Bulletin*,
912 *114*(3), 510–532. http://www.ncbi.nlm.nih.gov/pubmed/8272468

913 Rhodes, G. (2006). The evolutionary psychology of facial beauty. *Annual Review of*
914 *Psychology*, *57*, 199–226. https://doi.org/10.1146/annurev.psych.57.102904.190208

915 Sandberg, K., Timmermans, B., Overgaard, M., & Cleeremans, A. (2010). Measuring
916 consciousness: is one measure better than the other? *Consciousness and Cognition*,
917 *19*(4), 1069–1078. https://doi.org/10.1016/j.concog.2009.12.013

918 Satterthwaite, T. D., Ruparel, K., Loughead, J., Elliott, M. A., Gerraty, R. T., Calkins, M. E.,
919 Hakonarson, H., Gur, R. C., Gur, R. E., & Wolf, D. H. (2012). Being right is its own
920 reward: Load and performance related ventral striatum activation to correct responses

JNeurosci Accepted Manuscript

during a working memory task in youth. *NeuroImage*, *61*(3), 723–729. https://doi.org/10.1016/j.neuroimage.2012.03.060

Shang, J., Zhong, K., Hou, X., Yao, L., Shi, R., & Wang, Z. (2025). Invisible and Visible Processing of Facial Attractiveness in Implicit Tasks: Evidence From Event-Related Potentials. *PsyCh Journal*, *36*(8), 2865–2877. https://doi.org/10.1002/pchj.70014

Skora, L. I., Livermore, J. J. A., Dienes, Z., Seth, A. K., & Scott, R. B. (2023). Feasibility of unconscious instrumental conditioning: A registered replication. *Cortex*, *159*, 101–117. https://doi.org/10.1016/j.cortex.2022.12.003

Smith, A., Douglas Bernheim, B., Camerer, C. F., & Rangel, A. (2014). Neural activity reveals preferences without choices. *American Economic Journal: Microeconomics*, *6*(2), 1–36. https://doi.org/10.1257/mic.6.2.1

Smith, S. M., & Nichols, T. E. (2009). Threshold-free cluster enhancement: addressing problems of smoothing, threshold dependence and localisation in cluster inference. *NeuroImage*, *44*(1), 83–98. https://doi.org/10.1016/j.neuroimage.2008.03.061

Stein, T., Hebart, M. N., & Sterzer, P. (2011). Breaking Continuous Flash Suppression: A New Measure of Unconscious Processing during Interocular Suppression? *Frontiers in Human Neuroscience*, *5*(NOVEMBER). https://doi.org/10.3389/fnhum.2011.00167

Stockart, F., Schreiber, M., Amerio, P., Carmel, D., Cleeremans, A., Deouell, L. Y., Dienes, Z., Elosegi, P., Gayet, S., Goldstein, A., Halchin, A. M., Hesselmann, G., Kimchi, R., Lamy, D., Loued-Khenissi, L., Meyen, S., Micher, N., Pitts, M., Salomon, R., … Mudrik, L. (2025). Studying unconscious processing: Contention and consensus. *Behavioral and Brain Sciences*. https://doi.org/10.1017/S0140525X25101489

Tusche, A., Bode, S., & Haynes, J. D. (2010). Neural responses to unattended products predict later consumer choices. *Journal of Neuroscience*, *30*(23), 8024–8031. https://doi.org/10.1523/JNEUROSCI.0064-10.2010

Valério, D., Peres, A., Bergström, F., Seidel, P., & Almeida, J. (2025). Neural and behavioral similarity-driven tuning curves for manipulable objects. *Imaging Neuroscience*, *3*. https://doi.org/10.1162/imag_a_00482

Wolf, D. H., Gerraty, R. T., Satterthwaite, T. D., Loughead, J., Campellone, T., Elliott, M. A., Turetsky, B. I., Gur, R. C., & Gur, R. E. (2011). Striatal intrinsic reinforcement signals during recognition memory: Relationship to response bias and dysregulation in schizophrenia. *Frontiers in Behavioral Neuroscience*, *5*(NOVEMBER), 1–9. https://doi.org/10.3389/fnbeh.2011.00081

Yu, L. Q., Dana, J., & Kable, J. W. (2022). Individuals with ventromedial frontal damage display unstable but transitive preferences during decision making. *Nature Communications*, *13*(1), 1–10. https://doi.org/10.1038/s41467-022-32511-w

Zink, C. F., Pagnoni, G., Martin-Skurski, M. E., Chappelow, J. C., & Berns, G. S. (2004). Human Striatal Responses to Monetary Reward Depend On Saliency. *Neuron*, *42*(3), 509–517. https://doi.org/10.1016/S0896-6273(04)00183-7

JNeurosci Accepted Manuscript

Figure 1. Experimental procedure. (**A**) The experiment had three presentation conditions: a face suppressed by continuous flash suppression (CFS; Face + CFS), a uniform background (absent a face) suppressed by CFS (No Face + CFS), and a clearly visible face without suppression (Face + No CFS). The image of the brain with anaglyph glasses is a schematic illustration of the CFS setup and participants visual experience, and was made with ChatGPT4 (**B**) fMRI delayed match-to-sample task procedure: Jittered inter-trial-interval (ITI), face presentation, jittered inter-stimulus-interval (ISI), sample-to-match response (counterbalanced buttons for responses), perceptual awareness scale (PAS). (**C**) Post-fMRI task: Mean subjective attractiveness ratings for each face used in the experiment. Participants were only

JNeurosci Accepted Manuscript

presented with images of faces from the sex they were most attracted to. The faces are numbered from 1 to 12 from highest to lowest mean ratings and prefixed with a letter that indicates whether the face belonged to the preselected high, medium, or low attractiveness category. The face in the illustrations (A) and (B) is AI generated and used with permission from Generated Photos (https://generated.photos).

Figure 2. Behavioral results. The figure shows face identification sensitivity (d') (uncorrected p-values) and reaction time (log10-transformed) across seen and unseen conditions (FDR corrected p-values for 6 pairwise tests). * $p < .05$, ** $p \leq .01$, *** $p \leq .001$.

Figure 3. Face perception. (**A**) Regions of interest (ROI) for univariate (yellow) and multivariate (red) analyses for the fusiform face area (FFA). (**B**) Predictor coefficients for the subset of voxels that contributed to significant multivariate face decoding results. (**C**) Univariate FFA results for contrasts seen > absent and unseen > absent. (**D**) Multivariate decoding results for seen vs. absent, unseen vs. absent, and cross-decoding presence vs. absence across seen and unseen faces. Warm color indicates a positive, and cold color a negative, relationship with neural signal and the presence of a face. Each violin shows the kernel density distribution of individual data points. The central box spans the interquartile range with a horizontal line at the median and a filled circle marking the mean, whiskers extend to 1.5 times the interquartile range. P-values were FDR-adjusted separately within each test set: 5 tests against chance and 2 paired tests. * $p < .05$, ** $p \leq .01$, *** $p \leq .001$.

Figure 4. Subjective value (SV) processing. (**A**) Regions of interest (ROI) for univariate (yellow), multivariate (red), and both (green) analyses for the anterior ventral striatum (aVS) and ventromedial prefrontal cortex (vmPFC). (**B**) Predictor coefficients for the subset of voxels that contributed to significant multivariate SV prediction results. (**C**) Univariate results for linear parametric SV contrasts for seen and unseen faces. (**D**) Multivariate continuous

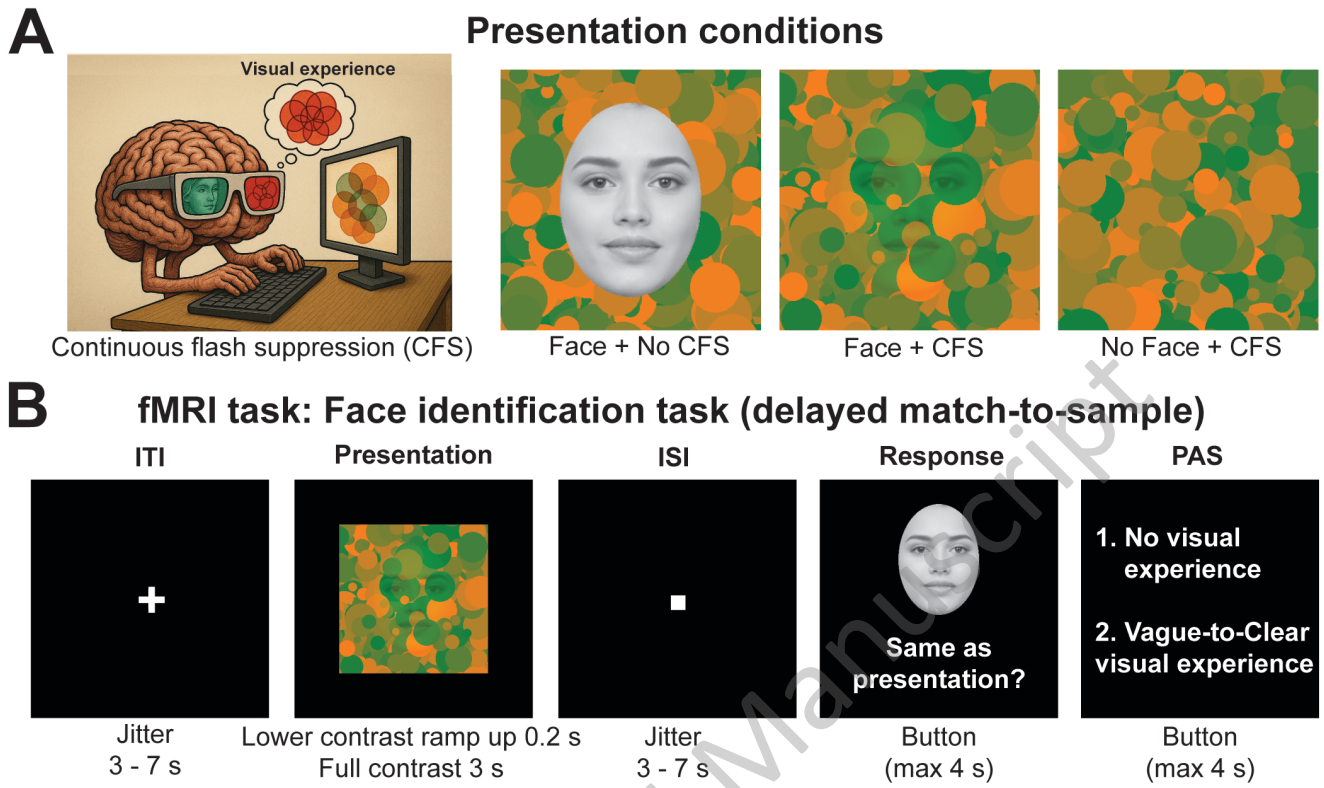
JNeurosci Accepted Manuscript

prediction results for SV from seen and unseen faces; and cross-decoding SV across seen and unseen faces. The lack of variability in aVS for seen SV is due to the models defaulting to the intercept model (retaining 0 voxels). Warm color indicates a positive, and cold color a negative, relationship with neural signal and higher SV. Each violin shows the kernel density distribution of individual data points. The central box spans the interquartile range with a horizontal line at the median and a filled circle marking the mean, whiskers extend to 1.5 times the interquartile range. P-values were FDR-adjusted separately within each test set: 10 tests against chance and 4 paired tests. * $p < .05$, ** $p \leq .01$, *** $p \leq .001$.

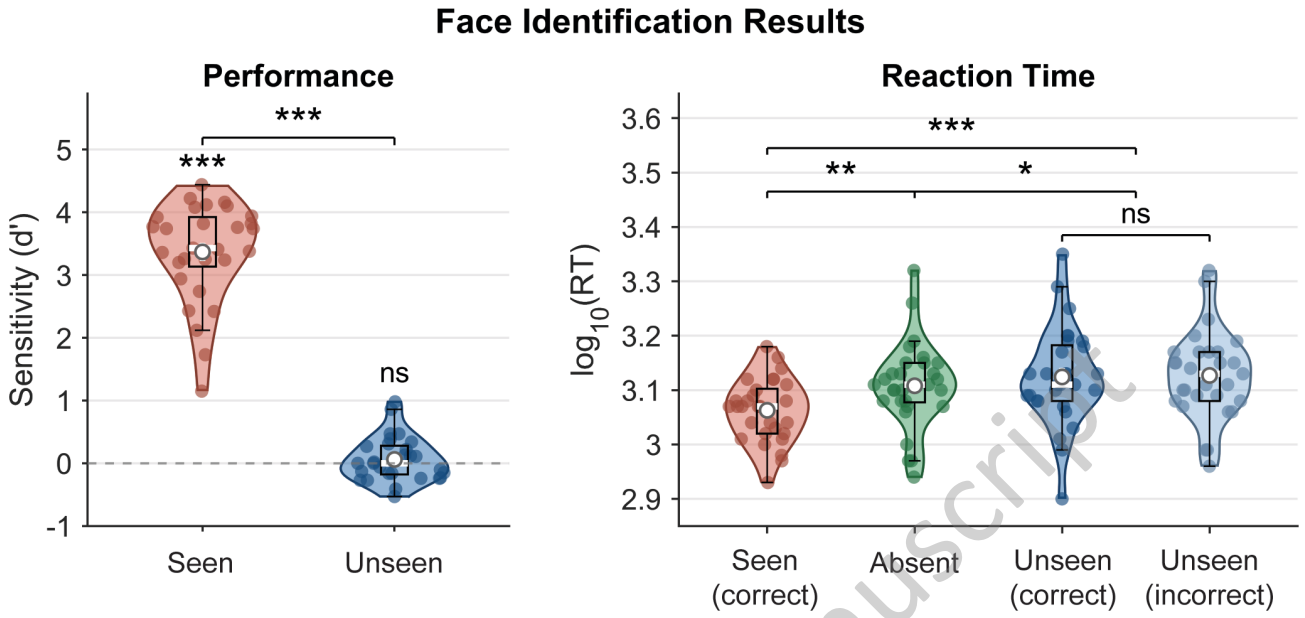
Figure 5. Relationship between face and subjective value (SV) signal. The scatter plots show the relationship between contrast estimates face > absent and parametric contrast estimates for facial attractiveness ratings. The red scatter plots in the left column show the relationships for seen faces and the right column with blue scatter plots show the relationship for unseen faces. The upper row shows the results for anterior ventral striatum (aVS) and the lower row the ventromedial prefrontal cortex (vmPFC). The line and shaded area show a Theil-Sen robust fit with a 95% bootstrap confidence interval (10,000 resamples). P-values are FDR corrected for four tests.

Figure 6. TFCE and FDR corrected whole-brain results. Univariate threshold free cluster enhancement (TFCE) adjusted and FDR corrected contrasts: (**A**) Linear parametric modulation results for subjective value (SV) of seen faces ($p < .05$, one-tailed). (**B**) Seen > absent face presentations ($p < .05$, one-tailed). (**C**) Seen > unseen face presentations ($p < .05$, two-tailed). The whole-brain contrasts with unseen SV or unseen > absent faces did not survive FDR corrections. Warm colors are positive and cold colors are negative statistical values.

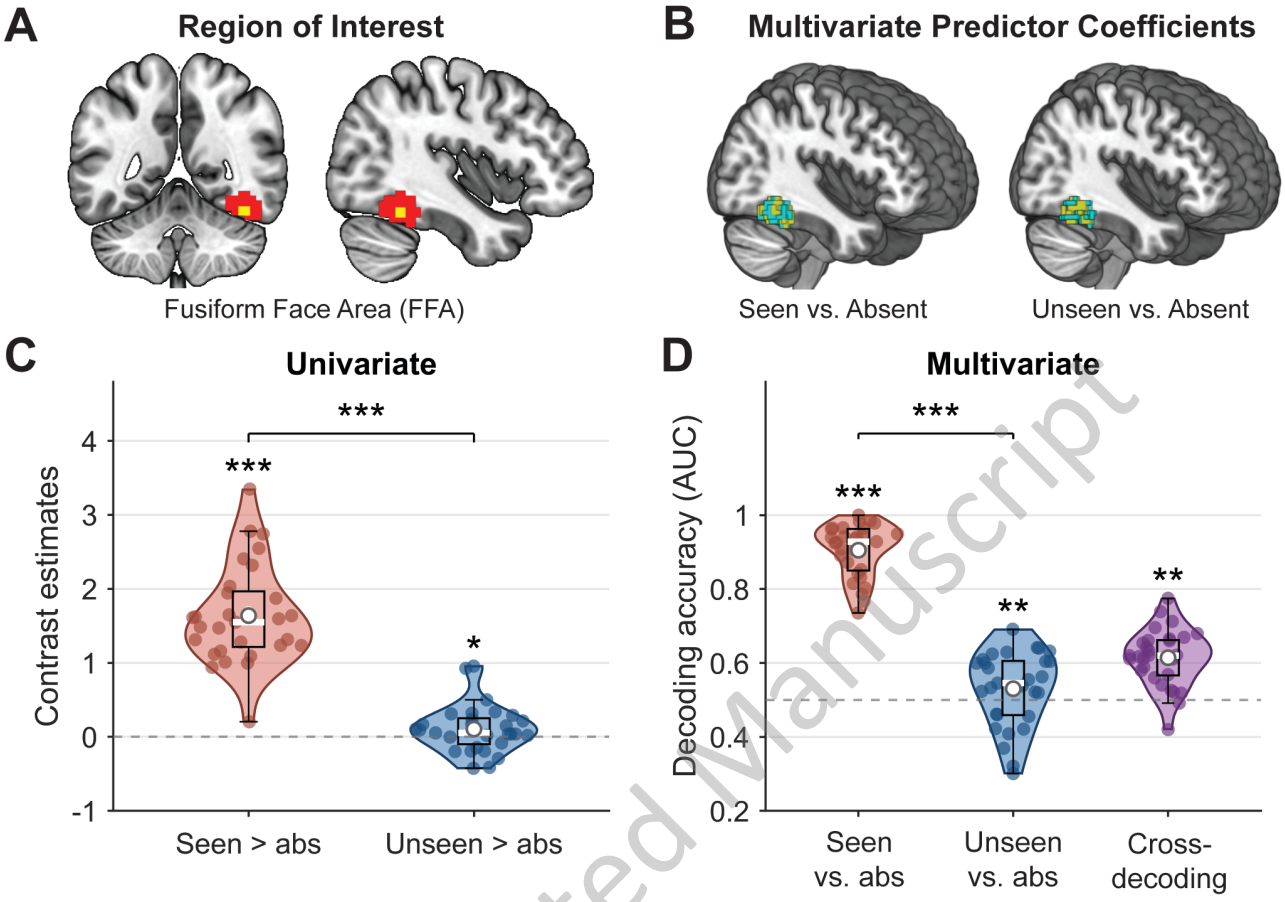
JNeurosci Accepted Manuscript



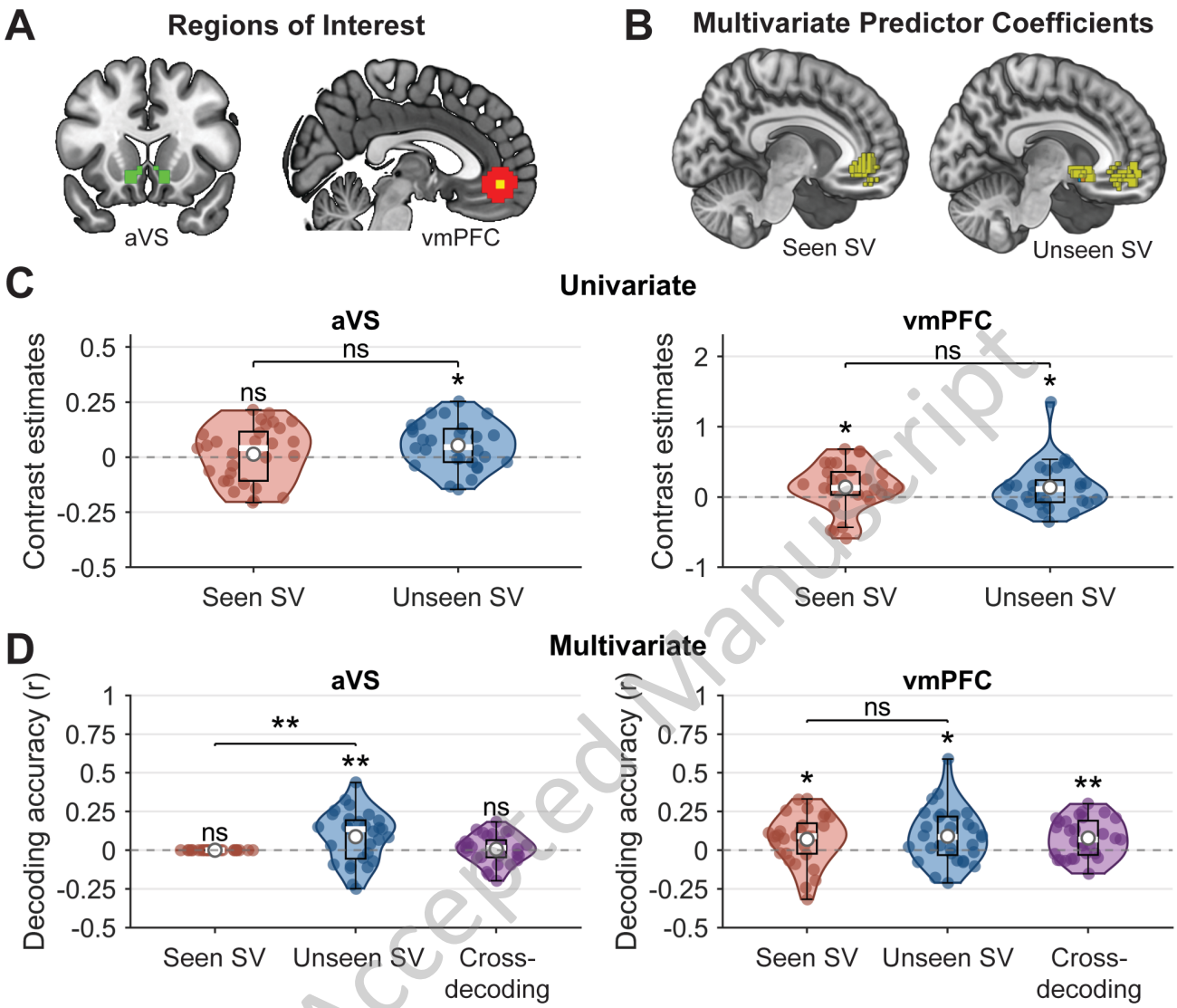
JNeurosci Accepted Manuscript



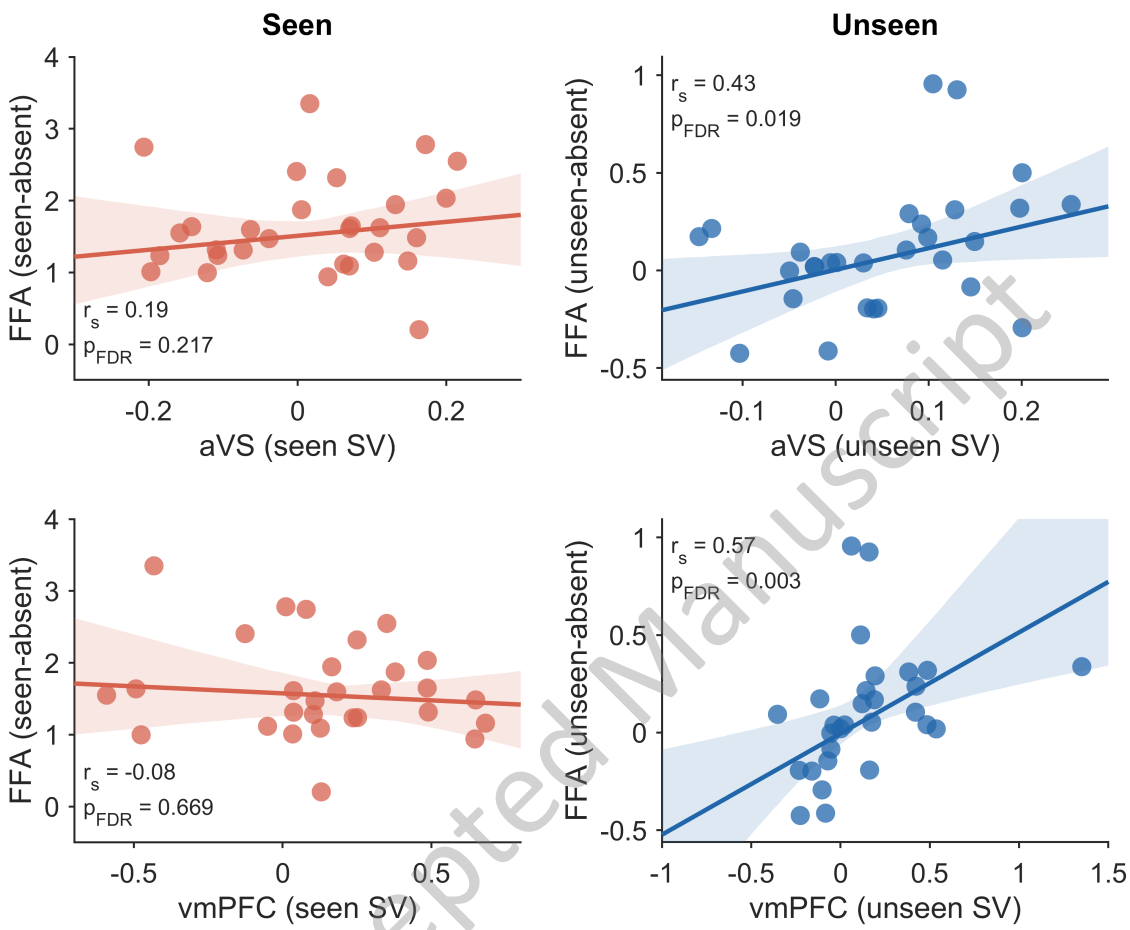
JNeurosci Accepted Manuscript



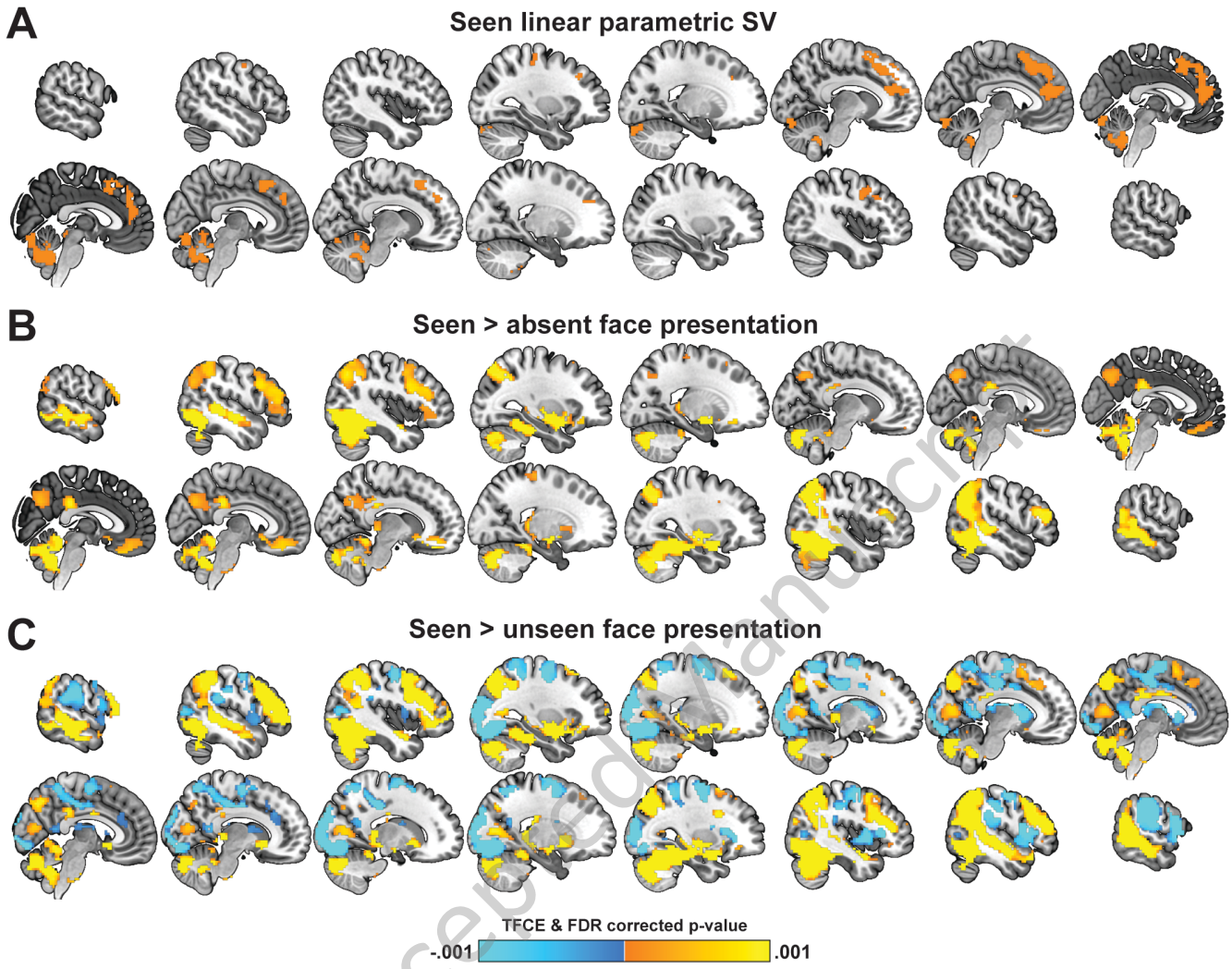
JNeurosci Accepted Manuscript



JNeurosci Accepted Manuscript



JNeurosci Accepted Manuscript



JNeurosci Accepted Manuscript